2013 IEEE/RSJ International Conference on
Intelligent Robots and Systems (IROS)
November 3-7, 2013. Tokyo, Japan

Complete Dynamic Modeling, Control and Optimization for an Over-Actuated MAV

Yangbo Long and David J. Cappelleri

***Abstract*— This paper presents an original configuration of a micro aerial vehicle (MAV), the Omnicopter. Two central counter-rotating coaxial propellers provide a major part of lift force, and three perimeter-mounted tiltable ducted fans are used to supplement the lift force, provide lateral forces and adjust its attitude. Different from traditional underactuated MAVs, the presence of the tilt-rotor mechanism, composed of three ducted fans and three servo motors, on the Omnicopter makes it over-actuated. The characteristic of over-actuation enables the Omnicopter's position dynamics to be decoupled from its attitude dynamics. Based on a complete description of its dynamic model derived using the Newton-Euler motion equations, we propose attitude and position controllers and control allocation for the Omnicopter MAV. Simulation and experimental results are shown to demonstrate its performance.**

I. INTRODUCTION

In recent years, the applications of multi-rotor unmanned aerial vehicles (UAVs) have widely diversified. Besides conventional MAV configurations, like quadrotors and helicopters, tilt-rotor type MAVs have been developed. Most of the famous tilt-rotor type UAVs for military use, like Bell Boeing V-22 Osprey [1], are mechanically complex since they employ a swashplate and differential rotor tilting to control pitch and yaw, respectively. Several research groups have also developed some tilt-rotor/wing type MAVs with simpler tilting and actuation designs [2], [3], [4], [5], [6].

In this paper, we introduce an original MAV configuration, named the Omnicopter MAV, composed of five rotors and three servo motors (see Fig. 1). The main characteristic of this configuration is that the attitude and translation dynamics are decoupled, such that we can design controllers for the two subsystems individually and fully control its 6 degrees of freedom (DOF) for more agility. For example, it can maintain zero roll and pitch attitude during lateral translation or arbitrarily orient the fuselage during hover.

Comparing with some other over-actuated multicopters in the literature, the Omnicopter has some potential advantages. In [7] and [8], the eight-rotor UAV's control inputs are linearly related to its motor input signals. However, the Omnicopter requires only five motors and three force vectoring mechanisms to generate desired lateral forces.In [5], the author proposed a quadrotor with tilting propellers. But the propellers' tilting will generate gyroscopic effects, which makes it more difficult to control. In contrast, the Omnicopter's design reduces possible gyroscopic effects.

Y. Long and D. Cappelleri are from Stevens Institute of Technology, 1 Castle Point on Hudson, Hoboken, NJ 07030, USA. D. Cappelleri is now at Purdue University, 585 Purdue Mall, West Lafayette, IN 47907. Email: ylong1@stevens.edu, dcappell@purdue.edu

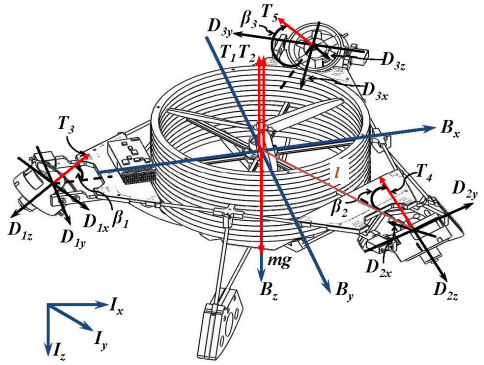

Fig. 1. Schematic and free-body diagram for Omnicopter MAV

From our previous work, in [9], we discussed about the modeling and attitude control of the Omnicopter using feedback linearization. In [10], we talked about the control of the Omnicopter under the fixed 90° ducted fan angle configuration. In [11], we designed and simulated control and control allocation algorithms for the Omnicopter under both the fixed 90° ducted fan angle and variable angle ducted fan configurations, and implemented these algorithms for the former configuration. In this paper, we improved the dynamic model by taking into account the aerodynamic drag effects due to the ducts and the gyroscopic effects due to the tilting of the surrounding fans. We also experimentally verified the lateral translation performance of the Omnicopter.

The outline of this paper is as follows: In Section II we develop a detailed mathematical nonlinear model of the Omnicopter. In Section III, for the zero attitude translation case, we present a backstepping based attitude controller and a standard PID position controller, and apply a pseudoinverse based optimization technique to allocate the control signals. Section IV presents some simulation results to illustrate the performance of the proposed control and allocation techniques. The platform setup and experiments are described in Section V, and finally concluding remarks based on all the presented work are given in Section VI.

II. OMNICOPTER DYNAMIC MODEL

In this section, we apply the Newtonian mechanics to model the Omnicopter. Let $\boldsymbol{I} = I_x,\ I_y,\ I_z$ denote the inertial frame, and $\boldsymbol{B} = B_x,\ B_y,\ B_z$ the aircraft body frame, with the z axes pointing downwards, as shown in Fig. 1.

A. Dynamic Model Based on Newton-Euler Equation

Using the Newton-Euler approach [12], we can derive the dynamics of a rigid body under external forces and torques applied to the rigid body

$$\begin{bmatrix} m\boldsymbol{I}_{3\times3} & \boldsymbol{0} \\ \boldsymbol{0} & \boldsymbol{J} \end{bmatrix} \begin{bmatrix} \dot{\boldsymbol{v}}^B \\ \dot{\boldsymbol{\omega}} \end{bmatrix} + \begin{bmatrix} \boldsymbol{\omega} \times m\boldsymbol{v}^B \\ \boldsymbol{\omega} \times \boldsymbol{J}\boldsymbol{\omega} \end{bmatrix} = \begin{bmatrix} \boldsymbol{f} \\ \boldsymbol{\tau} \end{bmatrix} \quad (1)$$

where $\boldsymbol{v}^B = [v_x \ v_y \ v_z]^T$ and $\boldsymbol{\omega} = [\omega_x \ \omega_y \ \omega_z]^T$ are the linear and angular velocities in the body frame, $\boldsymbol{J} = diag(I_{xx}, \ I_{yy}, \ I_{zz})$ is the inertial matrix and *m* mass, $\boldsymbol{f} = [f_x \ f_y \ f_z]^T$ and $\boldsymbol{\tau} = [\tau_x \ \tau_y \ \tau_z]^T$ are the force and torque vectors in the body frame.

We can expand (1) to obtain 6 independent equations of motion as the following

$$\begin{aligned} &m(\dot{v}_x - v_y\omega_z + v_z\omega_y + gs\theta) = f_x \\ &m(\dot{v}_y - v_z\omega_x + v_x\omega_z - gc\theta s\phi) = f_y \\ &m(\dot{v}_z - v_x\omega_y + v_y\omega_x - gc\theta c\phi) = f_z \\ &I_{xx}\dot{\omega}_x - (I_{yy} - I_{zz})\omega_y\omega_z = \tau_x \\ &I_{yy}\dot{\omega}_y - (I_{zz} - I_{xx})\omega_x\omega_z = \tau_y \\ &I_{zz}\dot{\omega}_z - (I_{xx} - I_{yy})\omega_x\omega_y = \tau_z \end{aligned} \quad (2)$$

where ϕ and θ stand for roll and pitch angles.

This is the dynamic model in the body coordinate frame. We can find that the translational equations of motion expressed in the body-fixed coordinate frame are pretty complex. Therefore, we prefer to express them in the inertial frame, while the rotational equations are expressed in the body-fixed frame. Finally, the full set of equations of motion are then obtained as the following

$$\begin{aligned} &\dot{\boldsymbol{\xi}} = \boldsymbol{v}^I \\ &m\dot{\boldsymbol{v}}^I = mg\boldsymbol{e}_3 + \boldsymbol{R}\boldsymbol{f} \\ &\dot{\boldsymbol{R}} = \boldsymbol{R}\boldsymbol{\omega}^\times \\ &\boldsymbol{J}\dot{\boldsymbol{\omega}} = -\boldsymbol{\omega}^\times\boldsymbol{J}\boldsymbol{\omega} + \boldsymbol{\tau} \end{aligned} \quad (3)$$

where $\boldsymbol{v}^I$ is the velocity in the inertial frame, $\boldsymbol{e}_3 = [0 \ 0 \ 1]^T$, the rotational matrix

$$\boldsymbol{R} = \begin{bmatrix} c\psi c\theta & c\psi s\theta s\phi - s\psi c\phi & c\psi s\theta c\phi + s\psi s\phi \\ s\psi c\theta & s\psi s\theta s\phi + c\psi c\phi & s\psi s\theta c\phi - s\phi c\psi \\ -s\theta & c\theta s\phi & c\theta c\phi \end{bmatrix} \quad (4)$$

where *c* = cos, *s* = sin and ψ is the yaw angle, and

$$\boldsymbol{\omega}^\times = \begin{bmatrix} 0 & -\omega_z & \omega_y \\ \omega_z & 0 & -\omega_x \\ -\omega_y & \omega_x & 0 \end{bmatrix} \quad (5)$$

B. External Forces and Torques

In the following, we derive the external forces and torques ($\boldsymbol{f}$ and $\boldsymbol{\tau}$) exerted on the Omnicopter. For convenience's sake, we attach three additional coordinate frames to the ducted fans of the Omnicopter, $\boldsymbol{D}_1 = D_{1x}, \ D_{1y}, \ D_{1z}$, $\boldsymbol{D}_2 = D_{2x}, \ D_{2y}, \ D_{2z}$ and $\boldsymbol{D}_3 = D_{3x}, \ D_{3y}, \ D_{3z}$. Therefore, the orientation of the ducted fans D_1, D_2 and D_3 with respect to the body frame, *B*, can be defined by the rotational matrices $\boldsymbol{R}_1$, $\boldsymbol{R}_2$ and $\boldsymbol{R}_3$, respectively, by

$$\begin{aligned} \boldsymbol{R}_1 &= \boldsymbol{R}_{D_{1y}}^{-(\frac{\pi}{2}-\beta_1)} = \begin{bmatrix} s\beta_1 & 0 & -c\beta_1 \\ 0 & 1 & 0 \\ c\beta_1 & 0 & s\beta_1 \end{bmatrix} \\ \boldsymbol{R}_2 &= \boldsymbol{R}_{D_{2z}}^{\frac{-2\pi}{3}}\boldsymbol{R}_{D_{2y}}^{-(\frac{\pi}{2}-\beta_2)} = \begin{bmatrix} -\frac{1}{2}s\beta_2 & \frac{\sqrt{3}}{2} & \frac{1}{2}c\beta_2 \\ -\frac{\sqrt{3}}{2}s\beta_2 & -\frac{1}{2} & \frac{\sqrt{3}}{2}c\beta_2 \\ c\beta_2 & 0 & s\beta_2 \end{bmatrix} \\ \boldsymbol{R}_3 &= \boldsymbol{R}_{D_{3z}}^{\frac{2\pi}{3}}\boldsymbol{R}_{D_{3y}}^{-(\frac{\pi}{2}-\beta_3)} = \begin{bmatrix} -\frac{1}{2}s\beta_3 & -\frac{\sqrt{3}}{2} & \frac{1}{2}c\beta_3 \\ \frac{\sqrt{3}}{2}s\beta_3 & -\frac{1}{2} & -\frac{\sqrt{3}}{2}c\beta_3 \\ c\beta_3 & 0 & s\beta_3 \end{bmatrix} \end{aligned} \quad (6)$$

where $\boldsymbol{R}_x^y$: x is the rotation axis and y the rotation angle.

1) Thrust Forces: The thrusts generated by the five rotors, T_1 to T_5, can be expressed in the body-fixed frame and the ducted-fan fixed frames as the following

$$\begin{aligned} &\boldsymbol{T}_1^B = [0 \ 0 \ T_1]^T, \ \boldsymbol{T}_2^B = [0 \ 0 \ T_2]^T; \\ &\boldsymbol{T}_3^{D_1} = [0 \ 0 \ T_3]^T, \ \boldsymbol{T}_4^{D_2} = [0 \ 0 \ T_4]^T, \ \boldsymbol{T}_5^{D_3} = [0 \ 0 \ T_5]^T. \end{aligned} \quad (7)$$

where T_i is the thrust that rotor *i* produces, which can be modeled as the following

$$\begin{aligned} &T_1 = -k_{T_1}\omega_1^2, \ T_2 = -k_{T_2}\omega_2^2; \\ &T_3 = -k_{T_3}\omega_3^2, \ T_4 = -k_{T_3}\omega_4^2, \ T_5 = -k_{T_3}\omega_5^2. \end{aligned} \quad (8)$$

where k_{T_1} and k_{T_2} are thrust factors of propeller 1 and 2, k_{T_3} is that of ducted fans, which depend on the blade geometry and can be experimentally tested. Thus, the thrust vector, $\boldsymbol{f}_t$, expressed in the body frame is given by

$$\begin{aligned} \boldsymbol{f}_t &= \boldsymbol{T}_1^B + \boldsymbol{T}_2^B + \boldsymbol{R}_1\boldsymbol{T}_3^{D_1} + \boldsymbol{R}_2\boldsymbol{T}_4^{D_2} + \boldsymbol{R}_3\boldsymbol{T}_5^{D_3} \\ &= \begin{bmatrix} k_{T_3}(\omega_3^2 c\beta_1 - \frac{1}{2}(\omega_4^2 c\beta_2 + \omega_5^2 c\beta_3)) \\ \frac{\sqrt{3}}{2}k_{T_3}(\omega_5^2 c\beta_3 - \omega_4^2 c\beta_2) \\ -k_{T_1}\omega_1^2 - k_{T_2}\omega_2^2 - k_{T_3}(\omega_3^2 s\beta_1 + \omega_4^2 s\beta_2 + \omega_5^2 s\beta_3) \end{bmatrix} \end{aligned} \quad (9)$$

2) Ram Drag Forces: The presence of the ducted fans also introduce aerodynamic drag effects. Ram drag is the result of the ducts and rotors changing the direction, and thus momentum, of the free-stream air. From [13], the induced air velocity inside each of the rotors is given by

$$V_i = \sqrt{-T_i/(2\rho S)} \quad (10)$$

where S is the area of the rotor disk and ρ the air density.

In the inertial frame, neglecting the presence of wind, the ram drag can be approximated as

$$\boldsymbol{f}_r = -(\rho S_p V_1 + \textstyle\sum_{i=3}^{5} \rho S_d V_i) \begin{bmatrix} \dot{\xi}_1 \\ \dot{\xi}_2 \\ 0 \end{bmatrix} \quad (11)$$

where the subscripts *p* and *d* represent propeller and ducted fan, respectively.

Because the central propellers provide approximately 60% of total lift force and ducted fans 40% at hover (i.e., $T_1 = -\frac{3}{10}mg$ and $T_i = -\frac{2}{15}mg$, *i* = 3, 4, 5), using (10), it can be expressed as the following

$$\boldsymbol{f}_r = -\lambda[\ \dot{\xi}_1 \ \dot{\xi}_2 \ 0\ ]^T \quad (12)$$

where $\lambda = \sqrt{0.15\rho S_p mg} + \sqrt{0.6\rho S_d mg}$ is constant.

The force vector, $\boldsymbol{f}$, in the body frame, is a combination of the thrusts and the drag forces, and can be expressed as

$$\boldsymbol{f} = \boldsymbol{f}_t + \boldsymbol{R}^T\boldsymbol{f}_r \quad (13)$$

where the right-hand side can be replaced by equations (9) and (12).

3) Thrust Imbalance and Counter Torques: From Fig., the distance from the gravity center to the ducted fan center is *l*. We can define distance vectors for the ducted fans, $\boldsymbol{OD}_1 = [-l \ 0 \ 0]^T$, $\boldsymbol{OD}_2 = [\frac{\sqrt{3}}{2}l \ \frac{1}{2}l \ 0]^T$ and $\boldsymbol{OD}_3 = [\frac{\sqrt{3}}{2}l \ -\frac{1}{2}l \ 0]^T$, in the body frame. Then, the torque vector exerted by ducted fan thrusts on the airframe is

$$\begin{aligned} \boldsymbol{\tau}_t &= \boldsymbol{R}_1\boldsymbol{T}_3^{D_1} \times \boldsymbol{OD}_1 + \boldsymbol{R}_2\boldsymbol{T}_4^{D_2} \times \boldsymbol{OD}_2 + \boldsymbol{R}_3\boldsymbol{T}_5^{D_3} \times \boldsymbol{OD}_3 \\ &= \begin{bmatrix} \frac{\sqrt{3}l}{2}k_{T_3}(\omega_5^2 s\beta_3 - \omega_4^2 s\beta_2) \\ \frac{l}{2}k_{T_3}(\omega_4^2 s\beta_2 + \omega_5^2 s\beta_3) - lk_{T_3}\omega_3^2 s\beta_1 \\ 0 \end{bmatrix} \end{aligned} \quad (14)$$

For the central propellers, as they rotate, they are subject to drag forces which produce counter drag torques around the B_z axis. For the ducted fans, the counter torques are eliminated due to the fins in their housings. The counter torque vector generated by the central propellers is

$$\boldsymbol{\tau}_c = \begin{bmatrix} 0 \\ 0 \\ k_{Q_1}\omega_1^2 - k_{Q_2}\omega_2^2 \end{bmatrix} \tag{15}$$

where k_{Q_1} and k_{Q_2} are drag factors.

4) Gyroscopic Torques: Since the servos rotate at a relatively low speed and due to the limited size of the ducts, we ignore the inertial effect introduced by the rotation of the ducted fans by the servos. As for the fast spinning ducted fan rotors, tilting the ducted fans around axes D_{1y}, D_{2y} and D_{3y} creates gyroscopic torques which are perpendicular to these axes and to the spin axes D_{1z}, D_{2z} and D_{3z}. They are expressed in the ducted-fan fixed frames as

$$\begin{aligned} \boldsymbol{\tau}_g^{D_1} &= -I_d\dot{\beta}_1\omega_3 D_{1x} \\ \boldsymbol{\tau}_g^{D_2} &= -I_d\dot{\beta}_2\omega_4 D_{2x} \\ \boldsymbol{\tau}_g^{D_3} &= -I_d\dot{\beta}_3\omega_5 D_{3x} \end{aligned} \tag{16}$$

where I_d is the inertia of ducted fans.

These torques can be transformed into the body frame by multiplying the above equations by $\boldsymbol{R}_1$, $\boldsymbol{R}_2$ and $\boldsymbol{R}_3$. Therefore, the gyroscopic torque vector in the body frame is

$$\begin{aligned} \boldsymbol{\tau}_g &= \boldsymbol{R}_1\boldsymbol{\tau}_g^{D_1} + \boldsymbol{R}_2\boldsymbol{\tau}_g^{D_2} + \boldsymbol{R}_3\boldsymbol{\tau}_g^{D_3} \\ &= I_d \begin{bmatrix} -\dot{\beta}_1\omega_3 s\beta_1 + \frac{1}{2}\dot{\beta}_2\omega_4 s\beta_2 + \frac{1}{2}\dot{\beta}_3\omega_5 s\beta_3 \\ \frac{\sqrt{3}}{2}\dot{\beta}_2\omega_4 s\beta_2 - \frac{\sqrt{3}}{2}\dot{\beta}_3\omega_5 s\beta_3 \\ -\dot{\beta}_1\omega_3 c\beta_1 - \dot{\beta}_2\omega_4 c\beta_2 - \dot{\beta}_3\omega_5 c\beta_3 \end{bmatrix} \end{aligned} \tag{17}$$

The complete expression of the external torque vector $\boldsymbol{\tau}$ with respect to the body frame $\boldsymbol{B}$ is

$$\boldsymbol{\tau} = \boldsymbol{\tau}_t + \boldsymbol{\tau}_c + \boldsymbol{\tau}_g \tag{18}$$

where the right-hand side can be replaced and explicitly expressed by equations (14), (15) and (17).

III. CONTROL DESIGN FOR ZERO ATTITUDE TRANSLATION

In this paper, we consider the case of zero attitude translation, and design and implement a position and attitude control system in a linear form. The original nonlinear model consisting of equations (3), (13) and (18) is very complex. In order to simplify the model for control design purpose, we neglect the gyroscopic torque, $\boldsymbol{\tau}_g$, which is reasonable considering the counter rotating central propellers and the ducted-fan blades with light inertia. Therefore, the external torques can be simplified into

$$\tilde{\boldsymbol{\tau}} = \begin{bmatrix} \tilde{\tau}_x \\ \tilde{\tau}_y \\ \tilde{\tau}_z \end{bmatrix} = \begin{bmatrix} \frac{\sqrt{3}l}{2}k_{T_3}(\omega_5^2 s\beta_3 - \omega_4^2 s\beta_2) \\ \frac{l}{2}k_{T_3}(\omega_4^2 s\beta_2 + \omega_5^2 s\beta_3) - lk_{T_3}\omega_3^2 s\beta_1 \\ k_{Q_1}\omega_1^2 - k_{Q_2}\omega_2^2 \end{bmatrix} \tag{19}$$

We can apply the small angle approximation, $\phi \approx 0$ and $\theta \approx 0$, the relation between Euler angles' derivatives and body angular speeds can be simplified to be

$$\begin{bmatrix} \dot{\phi} \\ \dot{\theta} \\ \dot{\psi} \end{bmatrix} = \begin{bmatrix} \omega_x \\ \omega_y \\ \omega_z \end{bmatrix} \tag{20}$$

The angular speed dynamics from (2) can be rewritten as

$$\begin{aligned} \dot{\omega}_x &= \tfrac{I_{yy}-I_{zz}}{I_{xx}}\omega_y\omega_z + \tfrac{1}{I_{xx}}\tilde{\tau}_x \\ \dot{\omega}_y &= \tfrac{I_{zz}-I_{xx}}{I_{yy}}\omega_x\omega_z + \tfrac{1}{I_{yy}}\tilde{\tau}_y \\ \dot{\omega}_z &= \tfrac{I_{xx}-I_{yy}}{I_{zz}}\omega_x\omega_y + \tfrac{1}{I_{zz}}\tilde{\tau}_z \end{aligned} \tag{21}$$

In order to further simplify the analysis, we neglect the high-order Coriolis terms in (21), and linearize it about the hovering operating point as the following

$$\begin{aligned} \dot{\omega}_x &= \tfrac{1}{I_{xx}}\tilde{\tau}_x \\ \dot{\omega}_y &= \tfrac{1}{I_{yy}}\tilde{\tau}_y \\ \dot{\omega}_z &= \tfrac{1}{I_{zz}}\tilde{\tau}_z \end{aligned} \tag{22}$$

A. Attitude Control

This section describes the development of an integral backstepping (IB) controller, which is similar to that described in [14] and [15]. The IB controller is composed of an outer attitude regulator and an inner angular velocity regulator, and implemented on the Omnicopter as discussed later in Sect. V-B. We start with roll by considering the tracking error $e_\phi = \phi^{des} - \phi$ and its dynamics

$$\dot{e}_\phi = \dot{\phi}^{des} - \omega_x \tag{23}$$

where the superscript, des, indicates the desired value, and the angular velocity ω_x is considered as a virtual control and designed to be

$$\omega_x^{des} = k_1 e_\phi + \dot{\phi}^{des} + k_2 \textstyle\int e_\phi dt \tag{24}$$

The above virtual control introduces the integral terms into the backstepping design, with k_1 and k_2 positive constants. The angular velocity tracking error is defined by

$$e_{\omega_x} = \omega_x^{des} - \omega_x \tag{25}$$

Using (24) and (25) we can obtain the derivative of e_{ω_x}

$$\dot{e}_{\omega_x} = \dot{\omega}_x^{des} - \ddot{\phi} = k_1\dot{e}_\phi + \ddot{\phi}^{des} + k_2 e_\phi - \ddot{\phi} \tag{26}$$

and rewrite the roll tracking error dynamics (23)

$$\begin{aligned} \dot{e}_\phi &= -k_1 e_\phi - k_2 \textstyle\int e_\phi dt + \omega_x^{des} - (\omega_x^{des} - e_{\omega_x}) \\ &= -k_1 e_\phi - k_2 \textstyle\int e_\phi dt + e_{\omega_x} \end{aligned} \tag{27}$$

Replacing $\ddot{\phi}$ in (26) by its linearized attitude dynamics (20) and (22), finally the control input, τ_x, appears in (28)

$$\dot{e}_{\omega_x} = k_1\dot{e}_\phi + \ddot{\phi}^{des} + k_2 e_\phi - \tfrac{1}{I_{xx}}\tilde{\tau}_x \tag{28}$$

The desired dynamics of the angular velocity tracking error is

$$\dot{e}_{\omega_x} = -k_3 e_{\omega_x} - k_4 e_\phi \tag{29}$$

which is obtained if the control input is designed to be

$$\begin{aligned} \tilde{\tau}_x = I_{xx}((k_4 - k_1^2 + k_2)e_\phi + (k_1 + k_3)e_{\omega_x} \\ -k_1 k_2 \textstyle\int e_\phi dt + \ddot{\phi}^{des}) \end{aligned} \tag{30}$$

where $k_3 > 0$ determines the convergence speed of the angular velocity loop and $k_4 > 0$.

Using (27) the above control law (30) can be transformed to be of a standard PID form

$$\begin{aligned} \tilde{\tau}_x = I_{xx}((k_1 k_3 + k_2 + k_4)e_\phi + (k_1 + k_3)\dot{e}_\phi \\ +k_2 k_3 \textstyle\int e_\phi dt + \ddot{\phi}^{des}) \end{aligned} \tag{31}$$

Following the same way, the controllers for pitch and yaw can be derived as

$$\begin{aligned} \tilde{\tau}_y = I_{yy}((k_5 k_7 + k_6 + k_8)e_\theta + (k_5 + k_7)\dot{e}_\theta \\ +k_6 k_7 \textstyle\int e_\theta dt + \ddot{\theta}^{des}) \end{aligned} \tag{32}$$

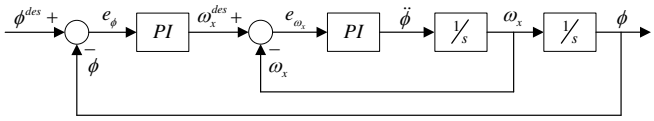

Fig. 2. Block diagram of integral backstepping controller

TABLE I

MODEL PARAMETERS

Parameter	Value	Parameter	Value
m	1.49 kg	k_{T_1}	$5.89\times10^{-8}\frac{N}{rpm^2}$
l^*	0.201 m	k_{T_2}	$5.30\times10^{-8}\frac{N}{rpm^2}$
I_{xx}	0.095 kg·m^2	k_{T_3}	$3.63\times10^{-9}\frac{N}{rpm^2}$
I_{yy}	0.082 kg·m^2	k_{Q_1}	$1.45\times10^{-9}\frac{N\cdot m}{rpm^2}$
I_{zz}	0.147 kg·m^2	k_{Q_2}	$1.45\times10^{-9}\frac{N\cdot m}{rpm^2}$

* Distance from ducted-fan center to propeller center

$$\tilde{\tau}_z = I_{zz}((k_9k_{11}+k_{10}+k_{12})e_\psi + (k_9+k_{11})\dot{e}_\psi + k_{10}k_{11}\int e_\psi dt + \ddot{\psi}^{des}) \tag{33}$$

As we can see from the derivation of the IB controller, it is essentially a cascaded PID controller, i.e., an outer-loop PI controller for attitude control and an inner-loop PI controller for angular velocity control. The block diagram of the controller is shown in Fig. 2.

B. Position Control

The translational dynamics in (3) can be expanded as

$$\begin{aligned} m\ddot{\xi}_1 + \lambda\dot{\xi}_1 &= \tilde{f}_x c\theta c\psi + \tilde{f}_y(c\psi s\theta s\phi - c\phi s\psi) \\ &\quad + \tilde{f}_z(s\phi s\psi + c\phi c\psi s\theta) \\ m\ddot{\xi}_2 + \lambda\dot{\xi}_2 &= \tilde{f}_x c\theta s\psi + \tilde{f}_y(s\psi s\theta s\phi + c\phi c\psi) \\ &\quad + \tilde{f}_z(c\phi s\psi s\theta - s\phi c\psi) \\ m\ddot{\xi}_3 &= mg - \tilde{f}_x s\theta + \tilde{f}_y c\theta s\phi + \tilde{f}_z c\theta c\phi \end{aligned} \tag{34}$$

where $\boldsymbol{f}_t = [\tilde{f}_x\ \tilde{f}_y\ \tilde{f}_z]^T = \boldsymbol{f} - \boldsymbol{R}^T\boldsymbol{f}_r$.

Using the attitude controller derived above and choosing proper gains, the closed-loop attitude dynamics will converge faster than the closed-loop translational dynamics. Because we are treating the zero attitude translation case, we can consider the attitude angles, $\psi \approx 0$, $\theta \approx 0$ and $\phi \approx 0$. Therefore, the above equations reduce to

$$\begin{aligned} m\ddot{\xi}_1 + \lambda\dot{\xi}_1 &= \tilde{f}_x \\ m\ddot{\xi}_2 + \lambda\dot{\xi}_2 &= \tilde{f}_y \\ m\ddot{\xi}_3 &= mg + \tilde{f}_z \end{aligned} \tag{35}$$

Then, the position controllers, $\tilde{f}_x$, $\tilde{f}_y$ and $\tilde{f}_z$, can be designed using classical PID control

$$\begin{aligned} \tilde{f}_x &= k_{P_x}(\xi_1^d - \xi_1) + k_{D_x}(\dot{\xi}_1^d - \dot{\xi}_1) + k_{I_x}\int_0^t(\xi_1^d - \xi_1)d\tau \\ \tilde{f}_y &= k_{P_y}(\xi_2^d - \xi_2) + k_{D_y}(\dot{\xi}_2^d - \dot{\xi}_2) + k_{I_y}\int_0^t(\xi_2^d - \xi_2)d\tau \\ \tilde{f}_z &= k_{P_z}(\xi_3^d - \xi_3) + k_{D_z}(\dot{\xi}_3^d - \dot{\xi}_3) \\ &\quad + k_{I_z}\int_0^t(\xi_3^d - \xi_3)d\tau - mg \end{aligned} \tag{36}$$

C. Control Allocation

$$\boldsymbol{a}^* = \arg\min_{\boldsymbol{a}}\{J|\tilde{\boldsymbol{u}} = \boldsymbol{B}\boldsymbol{a}\} \tag{37}$$

where $J = \|\boldsymbol{W}\boldsymbol{a}\|_2^2 = \sum_{i=1}^8 W_i a_i^2$, with a diagonal weighting matrix $\boldsymbol{W}$ composing of positive elements.

For the variable ducted fan configuration, 5 motor speeds (ω_1 to ω_5) and 3 servo angles (β_1 to β_3) need to be computed. The mapping equations between the actuator input $\boldsymbol{a} = [\omega_1^2\ \omega_2^2\ \omega_3^2\ \omega_4^2\ \omega_5^2\ \beta_1\ \beta_2\ \beta_3]^T$ and the virtual input $\boldsymbol{u} = [\tilde{f}_x\ \tilde{f}_y\ \tilde{f}_z\ \tilde{\tau}_x\ \tilde{\tau}_y\ \tilde{\tau}_z]^T$ are shown in (9), (14) and (15).

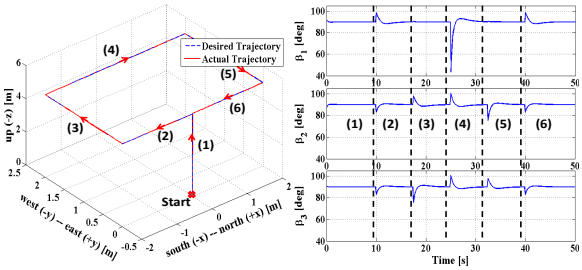

Fig. 3. 3D square path tracking (left) and ducted-fan servo angles using control allocation (right)

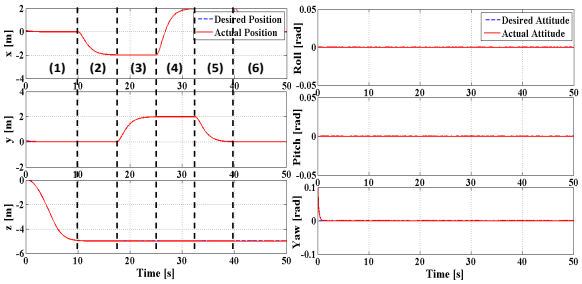

Fig. 4. Position and attitude performance for 3D square path tracking

Solving the actuator mapping equations for $\boldsymbol{a}$, while considering actuator constraints, amounts to performing constrained nonlinear programming. Since control allocation is to be performed in real-time, this may not be computationally feasible. One way to resolve this problem is to linearize the mapping locally around $\boldsymbol{a}_0$. Then we can arrive at

$$\boldsymbol{u}(\boldsymbol{a}) = \boldsymbol{u}(\boldsymbol{a}_0) + \frac{\partial \boldsymbol{u}}{\partial \boldsymbol{a}}|_{\boldsymbol{a}_0}(\boldsymbol{a} - \boldsymbol{a}_0) \tag{38}$$

which leads to the linear control allocation problem

$$\tilde{\boldsymbol{u}} = \boldsymbol{B}\boldsymbol{a} \tag{39}$$

where $\tilde{\boldsymbol{u}} = \boldsymbol{u}(\boldsymbol{a}) - \boldsymbol{u}(\boldsymbol{a}_0) + \boldsymbol{B}\boldsymbol{a}_0$ and the effectiveness matrix $\boldsymbol{B} = \frac{\partial \boldsymbol{u}}{\partial \boldsymbol{a}}|_{\boldsymbol{a}_0}$, $\boldsymbol{a}_0$ is picked as the previously applied control input, $\boldsymbol{a}(t-\delta)$, with δ as the step size.

The linearized mapping between the motor input, $\boldsymbol{a}$, and the control input, $\tilde{\boldsymbol{u}}$, is underdetermined, so we need to make a decision on how to achieve the forces and moments on the system. Here we choose an optimal actuator input $\boldsymbol{a}^*$ which achieves the desired control input $\tilde{\boldsymbol{u}}$ while minimizing the cost function, J

Then pseudoinverse based methods can be applied to solve the problem. After algebraic manipulation we get [16]

$$\boldsymbol{a} = \boldsymbol{W}^{-1}(\boldsymbol{B}\boldsymbol{W}^{-1})^\dagger\tilde{\boldsymbol{u}} = \boldsymbol{W}^{-2}\boldsymbol{B}^T(\boldsymbol{B}\boldsymbol{W}^{-2}\boldsymbol{B}^T)^{-1}\tilde{\boldsymbol{u}} \tag{40}$$

where † denotes the Moore-Penrose inverse.

Note that actuator constraints are not explicitly taken into account in the control allocation design. Instead, we truncate (40) by clipping those components that violate some constraints. However, in order to find an optimal solution, these constraints are needed to be considered. So we can formulate the control allocation problem as a linearly constrained quadratic programming problem [17], which is a topic of our future work.

TABLE II

CONTROL PARAMETERS

Parameter	Value	Parameter	Value
$k_{p,\phi}$	6.500	$k_{i,\phi}$	0.100
$k_{p,\theta}$	6.000	$k_{i,\theta}$	0.100
$k_{p,\psi}$	8.500	$k_{i,\psi}$	0.010
k_{p,ω_x}	0.305	k_{i,ω_x}	0.008
k_{p,ω_y}	0.285	k_{i,ω_y}	0.006
k_{p,ω_z}	0.330	k_{i,ω_z}	0.005

IV. SIMULATION

To demonstrate the capability of zero attitude translation of the Omnicopter, in this section we present simulation results of tracking a square path. The Omnicopter was configured to take off at the ground origin (0, 0, 0) with slight initial position and yaw errors, and then hover at 5 m height and track a square path of size 4×2 m^2 in the xy plane. Random white noise has been added to the feedback measurements. The model parameters, which are all experimentally determined and measured from CAD model, used in the simulation are shown in Table I.

From Fig. 3 and 4, we can find that the Omnicopter can track the path very well with zero attitude. This is not achievable for a traditional underactuated multicopter, since its position and attitude are coupled and a lateral translation depends on a change of attitude. We can also obtain the actuator control inputs (see Fig. 3 (right) for servo angles) using the control allocation technique.

V. EXPERIMENTS

A. Platform Setup

The control board, ArduPilot Mega, has the following main features: CPU module running at 16 MHz, 256K flash memory, 16 analog input channels, 6 serial ports, 8 fast PWM outputs. The on-board microprocessor, Atmega 2560, runs the control algorithms in real-time, therefore it reads the information provided by the IMU (inertial measurement unit), which is composed of a three-axis gyro, a three-axis accelerometer and a three-axis magnetometer.

For on-board sensing and position control, we are currently using a sonar sensor (MB1200, *MaxSonar*) to measure the distance from ground, and infrared sensors (GP2Y0A02YK0F, *Sharp*) to navigate the Omnicopter away from obstacles. The control board reads in the sonar and infrared sensors on its ADC port and also outputs PWM signals to the ESCs and servos. A GPS is incorporated for outdoor navigation. A component level breakdown of the major parts of the system and how they communicate with each other is depicted in Fig. 6.

An Omnicopter MAV prototype has been constructed as shown in Fig. 5. The prototype, including a 2700 mAh battery, weights 1.4 kg and measures 45 cm from a ducted fan hub to another. Custom mounts for each of the ducted fans were 3D printed out of ABS plastic. For actuation, we are using two 920 Kv motors to drive the two central propellers of size 10×7, and three 55 mm *AEO* ducted fans. The servo input signals are of standard 50 Hz, while the ESCs of the five motors receive inputs with a rate of up to 490 Hz.

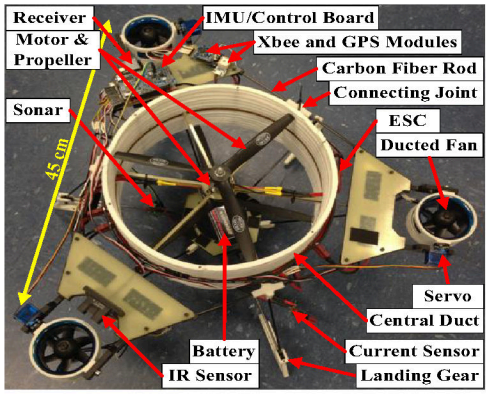

Fig. 5. Omnicopter MAV prototype

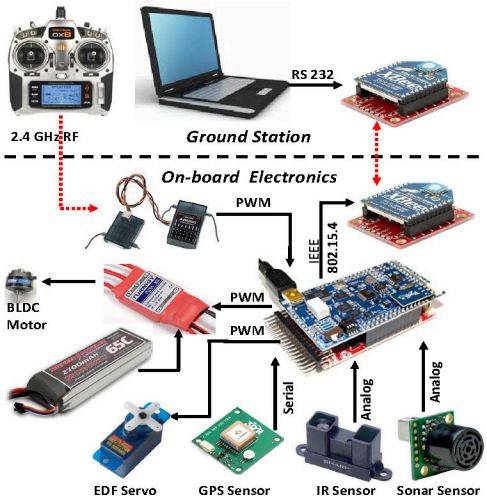

Fig. 6. System breakdown and communication between components

B. Experimental Results

In this section, the results of real-time experiments are presented. In the first experiment, the Omnicopter works under the fixed 90° degree ducted fan angle configuration. It first takes off from the ground and then hovers at a fixed set altitude. After hovering 30 seconds, it is controlled to track manual attitude inputs from a human operator via the transmitter. As we derived in Sec. III, the attitude loop is composed of an outer angle PI controller and an inner angular speed PI controller. The control gains are shown in Table II. From Fig. 7, we can find that the Omnicopter can hover well, with an attitude error of less than ±5 degrees. We can also find that there are some spikes when hovering. We believe this is because for the current prototype the carbon fiber frame is too flexible and the weight on each side of the aircraft is not perfectly balanced. Therefore, the pilot has to interfere in order to compensate for possible lateral drift. A new prototype, with more stiffness and better balance, is currently being constructed.

In the second experiment, the Omnicopter works under the variable angle ducted fan configuration. It translates forwards and backwards, with zero pitch angle. In Fig. 8 (top), the roll angle has several sharp spikes because we were manually adjusting the position of the robot by controlling roll. From Fig. 8 (middle and bottom) as well as the attached video,

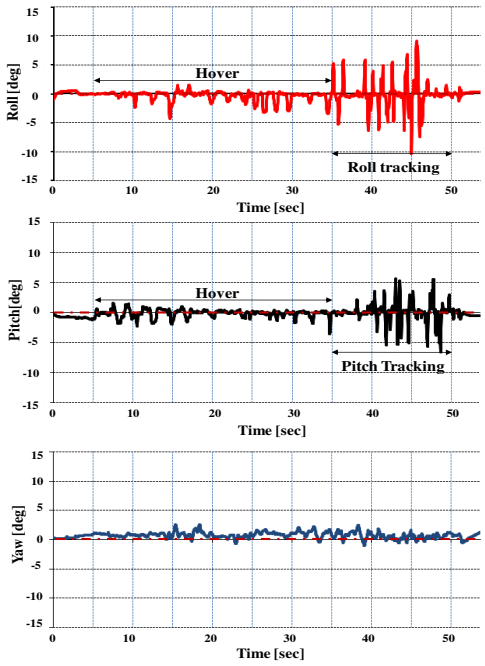

Fig. 7. Attitude control in the fixed 90° ducted fan angle configuration

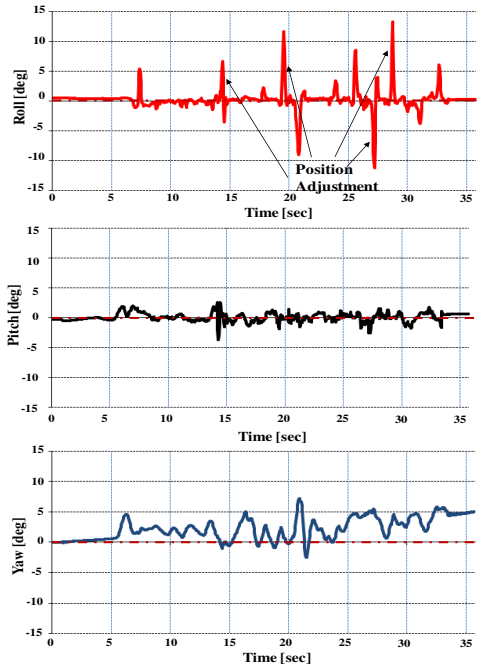

Fig. 8. Zero pitch translation in the variable angle ducted fan configuration

we can see that the Omnicopter can maintain almost zero pitch angle when translating horizontally. In addition, we qualitatively observed that in the variable angle ducted fan configuration, we can arrive at faster forward and backward flight comparing with the fixed 90° ducted fan configuration.

VI. CONCLUSIONS AND FUTURE WORK

In this paper, we have addressed the modeling and control of a novel multirotor aircraft, the Omnicopter. Its special actuation makes it possible to generate lateral forces and gain full controllability over its 6 DOF. Based on the complete dynamic model derived by applying Newton-Euler equations and multi-body system modeling, we presented control and optimization algorithms for zero attitude lateral translation. The proposed algorithms are verified and implemented by simulations and experiments on the prototype.

Having learned from our first prototype presented in this paper, we are developing the second generation prototype. Instead of making the frame using thin carbon fiber rods, we are going to simplify and 3D print the frame and as many parts as possible, to increase stiffness, robustness and manufacturability. We will also introduce a motion capture system for position control, and implement the control system using ROS (robot operating system). In this way, we can implement an adaptive backstepping based control algorithm [18] to achieve the proposed non-zero attitude hover and arbitrary trajectory tracking.

REFERENCES

[1] www.bellhelicopter.com.
[2] A. Sanchez, J. Escareno, O. Garcia, and R. L., Autonomous Hovering of a Noncyclic Tiltrotor UAV: Modeling, Control and Implementation, in *Proc. of the 17th IFAC Wold Cong.*, pp. 803808, 2008.
[3] F. Kendoul, I. Fantoni, and R. Lozano, Modeling and Control of a Small Autonomous Aircraft Having Two Tilting Rotors, in *IEEE Trans. on Robotics*, vol. 22, no. 6, pp. 12971302, 2006.
[4] K. T. Oner, E. Cetinsoy, E. Sirimoglu, C. Hancer, M. Unel, M. F. Aksit, K. Gulez, and I. Kandermir, Mathematical Modeling and Vertical Flight Control of a Tilt-Wing UAV, in *Turkish Journal of Electrical Engineering & Computer Science*, vol. 20, no. 1, 2012.
[5] M. Ryll, H. Buelthoff and P. Giordano, Modeling and Control of a Quadrotor UAV with Tilting Propellers, in *2012 IEEE Int. Conf. on Robotics and Automation*, 2012.
[6] F. Forte, R. Naldi, A. Serrani and L. Marconi, Control of Modular Aerial Robots: Combining Under- and Fully-Actuated Behaviors, in *IEEE Conf. on Decision and Control*, 2012.
[7] S. Salazar, H. Romero, R. Lozano and P. Castillo, Modeling and Real-Time Stabilization of an Aircraft Having Eight Rotors, in *J. Intell. Robot Syst.*, 54:455470, 2009.
[8] H. Romero, S. Salazar and R. Lozano, Real-Time Stabilization of an Eight-Rotor UAV Using Optical Flow, in *IEEE Trans. on Robotics*, vol. 25, no. 4, pp. 809817, 2009.
[9] Y. Long and D. Cappelleri, Design and Quaternion-Based Attitude Control of the Omnicopter MAV using Feedback Linearization, in *ASME Int. Design Engineering Technical Conf. (IDETC)*, 2012.
[10] Y. Long, S. Lyttle and D. Cappelleri, Linear Control Techniques Applied to the Omnicopter MAV in Fixed Vertical Ducted Fan Angle Configuration, in *ASME IDETC*, 2012.
[11] Y. Long and D. Cappelleri, Linear Control Design, Allocation, and Implementation for the Omnicopter MAV, in *IEEE Int. Conf. on Robotics and Automation*, 2013.
[12] R. Murray, Z. Li and S. Sastry, A Mathematical Introduction to Robotic Manipulation, *CRC Press, Boca Raton, FL*, 1994.
[13] R. Naldi, L. Gentili, L. Marconi and A. Sala, Design and Experimental Validation of a Nonlinear Control Law for a Ducted-fan Miniature Aerial Vehicle, in *Control Enginnering Practice*, vol. 18, no. 7, pp. 747-760, 2010.
[14] S. Bouabdallah, Design and Control of Quadrotors with Application to Autonomous Flying, *PhD Thesis*, Ecole Polytechnique Federale De Lausanne, 2007.
[15] F. Hoffmann, N. Goddemeier and T. Bertram, Attitude Estimation and Control of a Quadrocopter, in *The 2010 IEEE/RSJ International Conference on Intelligent Robots and Systems*, 2010.
[16] O. Harkegard, Backstepping and Control Allocation with Applications to Flight Control, *PhD Thesis*, Linkoping University, 2004.
[17] T. Johansen and T. Fossen, Control Allocation - A Survey, in *Automatica*, Nov, 2012.
[18] Y. Long, L. Wang and D. Cappelleri, Modeling and Global Trajectory Tracking Control for an Over-Actuated MAV, *Advanced Robotics*, to appear, 2013.